A radiation tolerant 4T pixel for space applications: layout and process optimization

Manuel Innocent
ON Semiconductor, Schaliënhoevedreef 20B, 2800 Mechelen, Belgium.
Manuel.Innocent@onsemi.com, tel +32 15 446 390, fax +32 15 448 780

Space applications require image sensors that are tolerant to the harsh radiation conditions outside the earth's atmosphere. This paper reports about an ongoing optimization experiment for radiation tolerant 4T pixels. The experiment is conducted in a 0.18µm CMOS image sensor process and involves optimization of both the layout and the process technology. The purpose of the experiment is to minimize the end-of-life dark current for a star tracker application while meeting all other electro-optical specifications. This implies tolerance to both ionizing dose and displacement damage.

Motivation

The presented radiation tolerant 4T pixel development is a next step in the long tradition of radiation tolerant image sensor designs that ON semiconductor has through the heritage of FillFactory and Cypress. The experiment is conducted in the framework of the ESA HAS3 sensor development project. The main application for the HAS3 is star tracking and it is intended to gradually replace its 3T pixel based predecessors HAS2 and STAR1000 The initial development of a 4T pixel for space applications was reported in [1]. Although it showed a significantly improved tolerance to ionizing dose compared to its 3T predecessor, it unfortunately did not show an improved tolerance to displacement damage. The consequence is that for the application the dark current increase resulting from displacement damage is currently the main concern and reduction of the sensitivity of that dark current to displacement damage is the main driver for the current experiment. Although dark current increase due to displacement damage is generally considered to be very fundamental, it can be influenced by design possibly at the expense of other specifications like full well charge and MTF.

Setup of the experiment

The beginning of life performance of any 4T pixel with the correct pitch and FWC meets the application requirements. The difficult part to guarantee is the end of life (EOL) performance and more specifically, the end of life dark current. End of life conditions for the HAS3 image sensor are 0.50 kGy TID and 1.8e10 p/cm2 equivalent 10MeV proton fluence. Our experiments go roughly a factor 2X further in TID and a factor 5X in proton fluence.
The experiment consists of 81 layout variants that allow checking the impact of layout choices in a side by side comparison. The vast majority of the variants use radiation tolerant layout techniques [5], but for reference some do not. The experiment also includes 9 process splits (baseline + 8 variants). The philosophy behind the choice of the process splits is as follows:
TID causes trapping of positive charges on the oxide to silicon interface. This is mainly a problem on the lower quality thicker STI and inter metal dielectric oxide, but less of an issue on the high quality thin gate oxide. This eventually causes an inversion channel to be created near the surface. This effect was suspected to cause the knee point of dark current versus TID data presented on the 2009 workshop [1]. Several process splits have been created with increasingly higher p-type doses near the surface. The purpose thereof is to push the point where an inversion channel is generated to a higher ionizing dose level.

The creation of displacement damage by high energetic particle radiation is fundamental and can hardly be influenced by design, but the impact on the sensor dark current can be influenced by limiting the volume of the photo diode depletion region and possibly also by limiting the electrical field over the depletion region. This drives another set of process splits. Eventually this results in variants on the 3 doping components that make up the photo diode. The photo diode top p-type implant, the photo diode n-type implant and the EPI doping level. These variants have different junction depths and have a different full well charge per unit area, which in its turn allows changing the photo diode area. Table 1 provides a short description of the process splits.

Measurement results

Figure 1 shows the spectral response of two different pixel variants in the baseline process split after proton radiation. The data is shown in the measured unit (V/s)/(W/m²) to prevent that the conclusions are obscured by e.g. an inaccurate calculation of the QE. It is clear that the variant shown on the left, that has very little STI, has less QE degradation after radiation than the variant shown on the right that has more STI. From this we can conclude that the degradation of the QE is almost entirely in the STI region while the active region is unaffected. The post TID spectral response data is not yet available, but since the equivalent ionizing dose of the 16MeV maximum fluence is already 0.4 kGy there will most likely not be any significant response degradation at the EOL ionizing dose.

At high displacement damage dose the full well charge (FWC) of the photo diode can reduce [4]. Vpin measurements can monitor these changes of the diode. Figure 2 shows the Vpin of the photo diodes of the different process splits before and after proton radiation. At the maximum tested radiation level there is no significant change to the Vpin of the diodes. Similarly, but not shown the Vpin shows no change at the maximum tested ionizing dose.

Figure 3 shows the dark current as function of the ionizing dose. For all splits except split 1 this relation is linear up to at least 1 kGy. Splits 2 and 4 have the lowest dark current but also have an unusable low FWC. Split 1 shows a knee point in its dark current similar to the one reported in [1]. This was attributed in [1] to an imperfect pinning at the top of the diode. This hypothesis still holds for this device since split 1 has an increased PDN dose with a standard PDP dose, which could result in the surface passivation inverting when positive charges accumulate at the oxide interface. Splits 6C and 6D have lower dark current than the baseline split, so those changes seem to be effective and can also be combined. Figure 4 shows the temperature behaviour of the post radiation dark current. Only split 6B has a different behaviour due to its different starting material.

Figure 5 shows the dark current as a function of proton fluence. In first order the trend is linear and the degradation is 10X worse at 16 Mev than at 62 MeV. There is a large difference between the degradation of the different process splits. Unfortunately, the post radiation dark current shows and inversely proportional relation with the full well charge per unit area. This means that changing the process split can be exchanged with changing the photo diode area in layout, but for a certain FWC there is only a very weak minimum in the dark current. Figure 6 and Figure 7 show the temperature behaviour of the dark current after the highest radiation level. The doubling temperature has increased which indicates more dark current is generated inside the diode depletion region. The different temperature behaviour of split 6B (both pre radiation and post TID) is absent in post proton data. This is consistent with the hypothesis that the dark current increase is due to damage inside the diodes depletion volume. It that scenario, the dark current due to the bulk becomes a relative small contribution for all splits.

Conclusion

The pixel we developed in the technology flavour we selected has no QE degradation at the EOL conditions for the application. The dark current increase after ionizing radiation is very limited and improves almost an order of magnitude over the results presented in [1]. Unfortunately, the EOL dark current increase due to displacement damage is too high for the application. A lot of effort will still be invested in finding the sweet spot in the massive amount of data. One path that we are further exploring is the use of an overflow photo gate to bring the FWC of diodes processed similar to split 2 or 4 to the FWC required by the application. This is described in more detail in [2].

split	Dev#	Description	Purpose
A0	1,2	Baseline	
1	3,4	High PDN dose (High FWC)	High FWC split allows to use a smaller PD area to meet the FWC spec.
2	5,6	High PDN/PDP dose, Shallow PDN	Small PD depletion volume due to shallower implant.
3	7,8	High PDP dose	Better surface passivation by higher dose, should be good for TID
4	9,10	Deep PDP	Better surface passivation by deeper junction, should be good for TID
5	11,12	Low PDN dose (Low FWC)	Low electric fields over the depletion regions
6A	13,14	Baseline	
6B	15,16	Baseline on P-well on N-epi wafers	No substrate dark current
6C	17,18	Baseline on high dose epi	Smaller PD depletion volume by shallower bottom depletion depth
6D	19,20	Baseline with high dose P-well	Better isolation between photo diode and STI, should be good for TID

Table 1: Description of the process spits

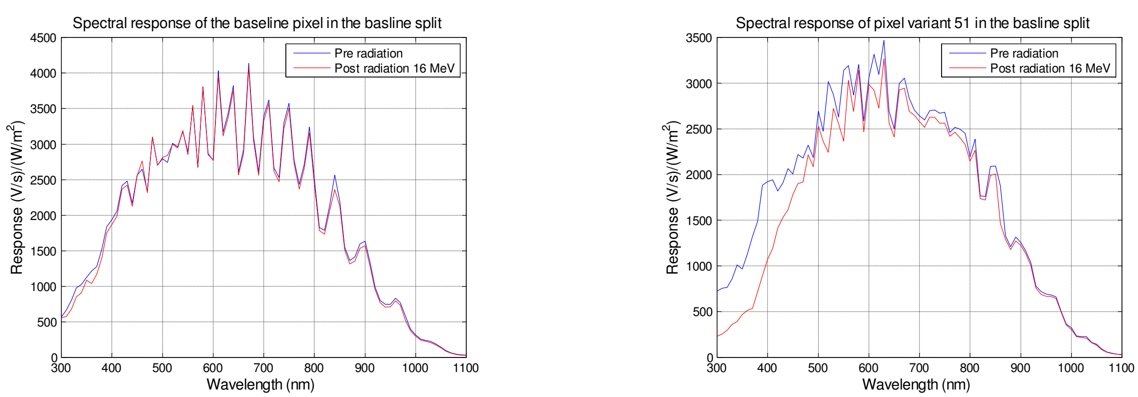

Figure 1: The spectral response of the baseline pixel variant (with little STI) and of another pixel layout variant (with more STI) in the same baseline process split. The baseline variant (left) is almost unchanged (perhaps slight degradation in the UV), while the other variant (right) is highly degraded in the blue after the worst case test condition of a fluence of 1e11 p/cm² with an energy of 16 MeV.

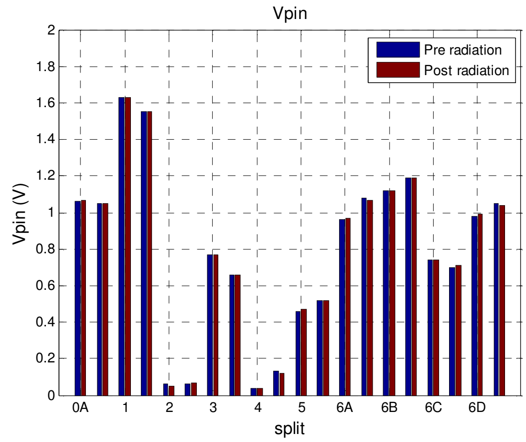

Figure 2: Vpin of two samples per split before and after proton radiation. The odd samples are radiated with 16 MeV protons, the even samples with 62 MeV protons. The Vpin differences between the two samples of the same split are larger than the change after radiation. The Vpin is basically unchanged after the maximum fluence and this for both tested proton energies.

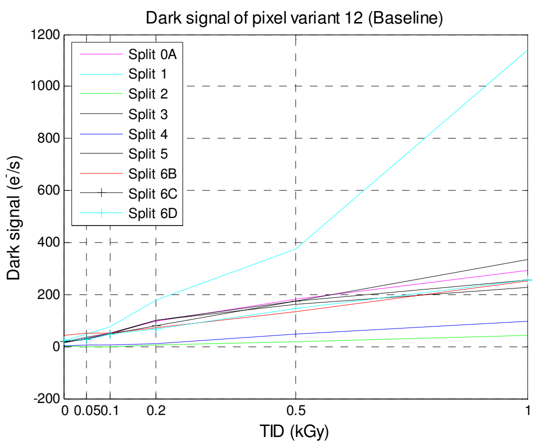

Figure 3: Post TID dark current of the baseline pixel for the different process splits measured in between the radiation steps. Measurements were at uncontrolled temperature, estimated to be 25°C. All splits except split 1 (which already has the highest dark current) have the dark signal increase linearly with TID up to atl least 1 kGy. Split 1 has a knee point before 1 kGy similar to data reported in [1]

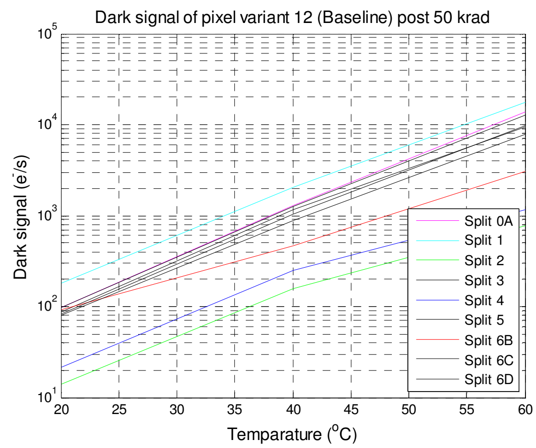

Figure 4: Post TID dark current of the baseline pixel for the different process splits as a function of temperature. All splits except split 6B have a doubling temperature close to 6°C. Split 6B has a slower increase due to its P-well on N-epi starting material that does not collect substrate dark current. Unfortunately, the dark current at 20°C is not better than the standard wafers and the QE of the sensor is significantly lower on this material.

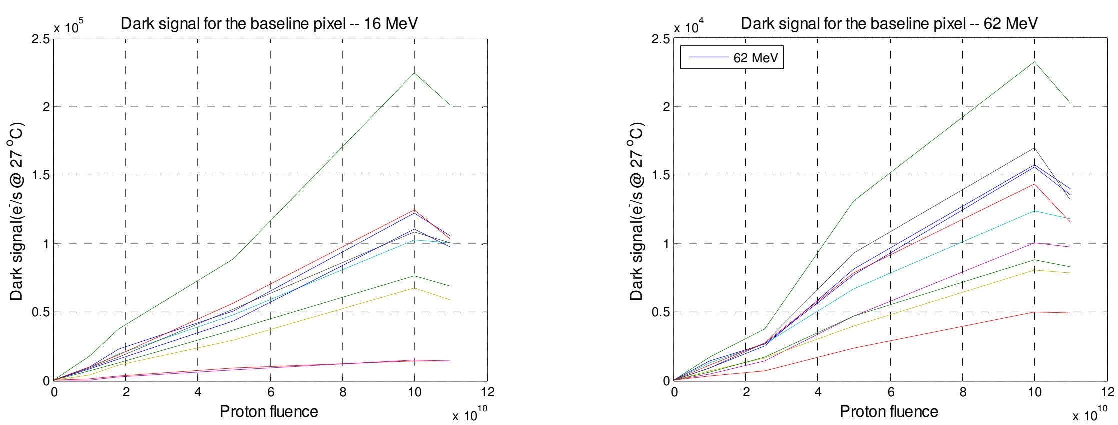

Figure 5: Post proton radiation dark current of the baseline pixel for the different process splits measured in between the radiation steps. Measurements were at uncontrolled temperature, estimated to be 27°C. The last point is measured 3 days after the last radiation step and shows some room temperature annealing. Notice the 10x different y-scale of the 2 graphs.

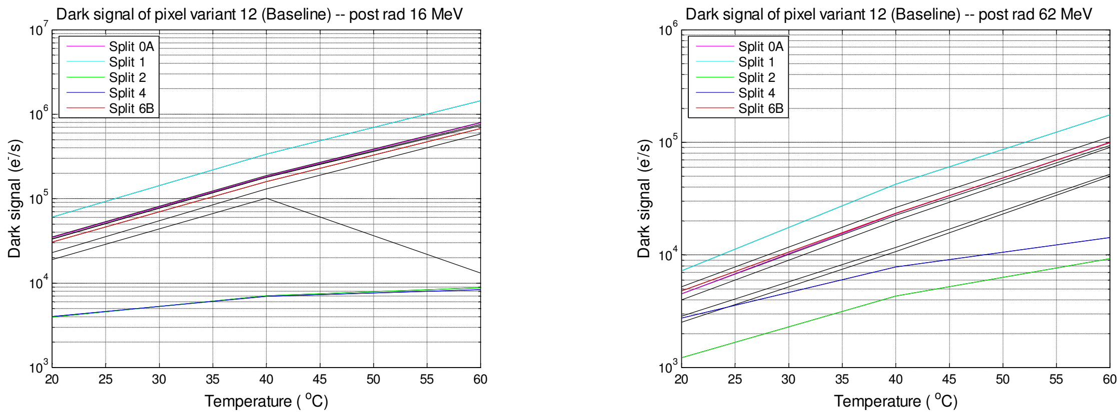

Figure 6: Post radiation dark current of the baseline pixel variant over the different process splits after the worst case test condition of a fluence of 1e11 p/cm² with an energy of 16 MeV for the left graph and 62 MeV for the right graph. Split 0A is the baseline split. Splits 2 and 4 show the lowest dark current, but have a very low FWC.

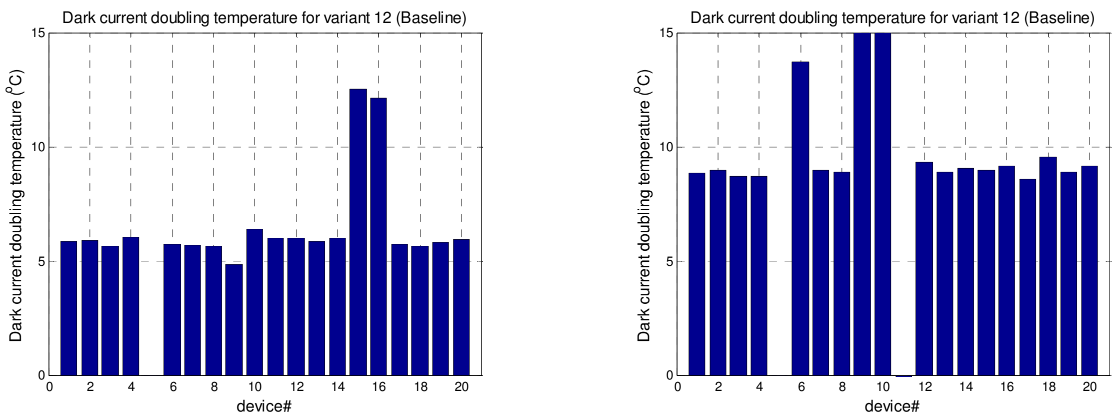

Figure 7: Dark current doubling temperature of all the samples before radiation and after the last radiation step. There are two samples for each process split. The odd samples are radiated with 16 MeV protons, the even samples with 62 MeV protons. Samples 15 and 16 (split 6B) have a fundamentally different starting material than all other splits which causes the initially different temperature behaviour, but after proton radiation this difference disappears. Splits 2 and 4 (samples 5, 6, 9 and 10) have inaccurate measurements due to the low FWC.

Technology	0.18µm CMOS image sensor process
Array size	180x144 in 81 pixel variants
Supply voltage	3.3V
Pixel type	4T pinned diode
Shutter type	Rolling shutter
Pixel size	11.25 µm x 11.25 µm
Pixel saturation charge	120ke^{-} target, most variants are higher
Output swing	1.6V
Radiation level EOL application	0.50 kGy TID 1.8e10 p/cm2 equivalent 10MeV proton fluence 2.5e10 p/cm2 equivalent 62MeV proton fluence
Radiation level EOL experiment	1 kGy TID 1e11 p/cm2 16 MeV 1e11 p/cm2 62 MeV

Table 2: key specifications

[1] M. Innocent, "A radiation tolerant 4T pixel for space applications," in Proc. IISW, 2009.
[2] Yannick De Wit, and Manuel Innocent, "An overflow photo-gate enables high FWC and improved proton radiation tolerance in CMOS pixels," in Proc. IISW, 2013.
[3] V. Goiffon et al., "Radiation Effects in Pinned Photodiode CMOS Image Sensors: Pixel Performance Degradation Due to Total Ionizing Dose," IEEE Trans. Nucl. Sci., vol. 59, pp. 2878–2887, Dec. 2012.
[4] C. Virmontois, V. Goiffon, F. Corbière, P. Magnan, S. Girard, and A.Bardoux, "Displacement Damage Effects in Pinned Photodiode CMOS Image Sensors," IEEE Trans. Nucl. Sci., vol. 59, pp. 2872–2877, Dec. 2012.
[5] H. L. Hughes, and J. M. Benedetto, "Radiation Effects and Hardening of MOS Technology: Devices and Circuits," IEEE Trans. Nucl. Sci., vol. 50, pp. 500–521, Jun. 2003.
[6] Jan Bogaerts, Bart Dierickx, Guy Meynants, and Dirk Uwaerts, "Total Dose and Displacement Damage Effects in a Radiation-Hardened CMOS APS," IEEE Trans. Nucl. Sci., vol. 50, pp. 84–90, Jan. 2003.
[7] Padmakumar R. Rao, Xinyang Wang, Adri J. Mierop, and Albert J.P. Theuwissen, "Gamma-Ray Irradiation Effects on CMOS Image Sensors in Deep Sub-Micron Technology," in Proc. IISW, 2007.